Article ID: 1000-324X(2015)08-0891-06 **DOI:** 10.15541/jim20150035

TiO_2 Nanowires Infiltrated with Graphene-decorated Mesoporous TiO_2 for Enhanced Dye-sensitized Solar Cell

CHEN Ang-Ran[1], ZHAO Wei[1], CUI Hou-Lei[1], ZHI Jian[1], HUANG Fu-Qiang[1, 2]

(1. CAS Key Laboratory of Materials for Energy Conversion, Shanghai Institute of Ceramics, Chinese Academy of Sciences, Shanghai 200050, China; 2. Beijing National Laboratory for Molecular Sciences, Beijing 100871, China)

Abstract: Novel hybrid dye-sensitized solar cells (DSSCs) were fabricated and characterized, employing a composite photoanode of TiO_2 nanowires infiltrated with graphene-decorated mesoporous TiO_2. Combining the merits of the high dye loading of mesoporous TiO_2, high light harvesting capability with the carrier transport of TiO_2 nanowires and the high electron collection efficiency from graphene, the overall performance of such photoanode was significantly improved. The obtained DSSCs showed a power conversion efficiency of up to 7.58%, about 1.5 times higher than the pristine TiO_2 nanowires, which was quite competitive compared with the similar 1D structured photoanode of DSSCs.

Key words: DSSCs; TiO_2 nanowires; mesoporous TiO_2; graphene

Among the many photovoltaic technologies, DSSCs have attracted tremendous attention as a promising alternative to the conventional silicon photovoltaic due to their low production cost and high conversion efficiencies[1-4]. A number of factors determines the overall conversion efficiency of DSSCs. Among them, the structural and physical properties of the anode materials are predominant[5]. Anatase TiO_2 nanoparticle (NP) film is an excellent starting photoelectrode for DSSCs due to its easy fabrication, minimal cost, and controllable over light scattering[6-8]. Recently, the one-dimensional (1D) semiconductor photoelectrode has drawn a lot of attention because of its merit of accelerated electron transport[9-12]. The NPs can provide high specific surface area for the dye adsorption, while the 1D nanomaterial can enhance the photogenerated electron transport. So far, there have been several investigations on this system, including TiO_2 NWs/NP and ZnO NWs/ NP composite solar cells[13-16]. However, owing to the loose packed structures and relatively low electrical conductivity of TiO_2 NPs, the electron transfer among the NPs, as well as between 1D NWs and NPs are limited[17-18]. Graphene, due to its high mobility up to 10^6 $cm^2/(V•s)$, high specific surface area reaching 2630 m^2/g and tunable band gap[19-20], it is expected that graphene would be an ideal additive material in photoanode to improve the property of DSSC.

In this work, 1D TiO_2 NWs (denoted as TNWs) were infiltrated with mesoporous TiO_2 (denoted as MT) decorated by reduced graphene oxide(RGO) (denoted as GMT) by multi-step evaporation induced self-assembly (EISA) process, and the hybrid composite (denoted as TNWs/GMT) film was obtained. TNWs/MT film as the comparison was obtained by the same way using MT instead of GMT. Such hybrid photoanode exhibits not only improved BET area but also outstanding electron transport property. Using TNWs/GMT with a thickness of about 2.5 μm as anode materials, the fabricated DSSCs showed a power conversion efficiency of up to 7.58 %, which is significantly improved over TNWs/MT (6.00%), and is quite competitive compared with the similar structured photoanode of DSSCs.

1 Experiments

1.1 Hydrothermal synthesis of TiO_2 nanowire (TNWs)

In a typical synthesis, 15 mL deionized water was mixed with 15 mL concentrated hydrochloric acid (37wt%) to reach a total volume of about 30 mL in a Teflon-lined stainless steel autoclave (50 mL volume). The mixture was stirred at ambient conditions for 5min before the addition of 0.5 mL of titanium butoxide (97wt%). After stirring for another 5 min, several pieces of FTO substrates were placed in parallel with the wall of the Teflon-liner. The hydrothermal synthesis was conducted at 180℃ for 6 h in

Received date: 2015-01-20; **Modified date:** 2015-03-26; **Published online:** 2015-04-20
Foundation item: National Natural Science Foundation of China (91122034, 51125006, 61376056, 61204072); Science and Technology Commission of Shanghai (13JC1405700, 14520722000)
Biography: CHEN Ang-Ran(1990-), male, candidate of PhD. E-mail: chenangran@student.sic.ac.cn
Corresponding author: HUANG Fu-Qiang, professor. E-mail: huangfq@mail.sic.ac.cn; ZHI Jian, phD. E-mail: jian.zhi@outlook.com

an oven. After synthesis, the autoclave was cooled to room temperature naturally. The post-synthesis sample was rinsed extensively with deionized water and allowed to dry in ambient air, annealed in air at 500℃ for 1 h in a furnace.

1.2 Preparation of mesoporous TiO_2 decorated by reduced graphene oxide (GMT) precursor solution

GMT precursor solution was prepared at room temperature in the following way: 1.26 g of poly (ethylene oxide)-b-poly (propylene oxide)-b-poly (ethylene oxide) triblock copolymer Pluronic F127 ($EO_{106}PO_{70}EO_{106}$) was dissolved in 22 g of pure ethanol and mixed with a precursor solution (prepared by mixing 3.36 g of 37wt% hydrochloric acid and 1.5 g deionized water); after stirring for 1 h, 5.68 g of titanium tetra isopropoxide (Ti (OCH $(CH_3)_2)_4$; TTIP) was added to the solution dropwise and the mixture was stirred for another 2 h after being mixed with 5 mg (1wt% TiO_2) reduced graphene oxide (RGO) which was synthesized by modified Hummers method[21].

1.3 Fabrication of TNWs/MT and TNWs/GMT photoanode

Finally, with the dip-coating technology the rutile TNWs FTO substrate were immersed into GMT precursor solution, then dried under 60% humidity conditions for 8 h and annealed at 120℃ for 30 min. Subsequently, the same procedure was repeated for another 4 times and the sample was calcinated at 350℃ for 3 h in air, to remove the F127 triblock copolymer template. The hybrid composite (TNWs/GMT) film was obtained. TNWs/MT film was obtained as the same way with pure MT precursor solution without reduced graphene oxide. More information about the experiment was written in support information.

2 Results and discussion

The cross-sectional morphology of bare TNWs was investigated by scanning electron microscope (SEM), as shown in Fig. 1(a). It is clear that the nanowires grow almost perpendicularly from the substrate with the length of 2.5 μm and width of 35 nm, similar to those shown in literature [22]. What's more, after first cycle infiltration process, GMT composites (1wt% graphene amount) was grown in the interstice between TNWs, as shown in Fig. 1(b). The well-defined mesoporous TiO_2/graphene nanost- ructures among TNWs indicated that the graphene not only provided a large surface for the nucleation of TiO_2 nanoparticles but also inhibited their aggregation[23]. Figure 1(c) shows the top-view image of the film in Fig. 1(b). Obviously, the loose packed TNWs were interconnected

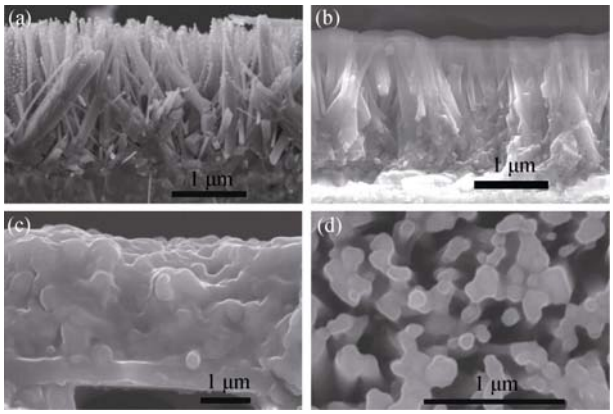

Fig. 1 Cross-sectional FESEM images of TNWs (a), cross-sectional (b) and top-sectional (c) FESEM of TNWs/GMT after one cycle infiltration, and cross-sectional FESEM of TNWs/GMT after 5 cycles infiltration (d)

with each other through GMT composites. However, due to the insufficient amount of mesoporous TiO_2/graphene in one cycle infiltration process, there are still some free spaces between TiO_2 NWs, which may inhibit the charge transportation and light scattering. To avoid this, multi-step infiltration process is needed in our systems. Figure 1(d) shows the morphology of TNWs/GMT film after 5-cycle infiltration. The TNWs were densely covered with GMT composites. No obvious large spaces exist in the film, which is beneficial for the photogenerated electron transfer[16]. Figure S1 shows the TEM image of the infiltrated GMT powder sample. A two-dimensional hexagonal pore structure with the average pore size of about 10 nm can be observed. Such highly porous and sponge-like microstructures are particularly beneficial for light harvesting[24]. From the TEM image, it is clear that RGO was incorporated into the TiO_2 film and mixed with a large number of TiO_2 nanoparticles. No apparent aggregation was observed, which indicated that the TiO_2 nanoparticles could disperse uniformly on or between the RGO sheets.

Figure 2(a) shows the XRD patterns of bare TNWs sample and naked FTO substrate. Clearly, TNWs are tetragonal rutile structure (JCPDS. 21-1276); the enhanced (002) peak indicates the nanowire is well crystallized and grows perpendicular to the substrate. Rutile-phase TiO_2 has been reported to exhibit lower efficiency than the anatase phase[25]. The close packing nature of rutile phase, which leads to the lower specific surface area[26]. Moreover, electron transport is relatively faster in the anatase phase than the rutile phase, as anatase phase has higher conduction-band edge energy[27]. Hence, anatase is the preferred phase for efficient functioning of the DSSC. Figure 2(b) shows the XRD patterns of pure mesoporous TiO_2 (MT) and GMT composites samples. It can be seen that most diffraction peaks of two samples are indexed to the anatase structure of TiO_2, which is

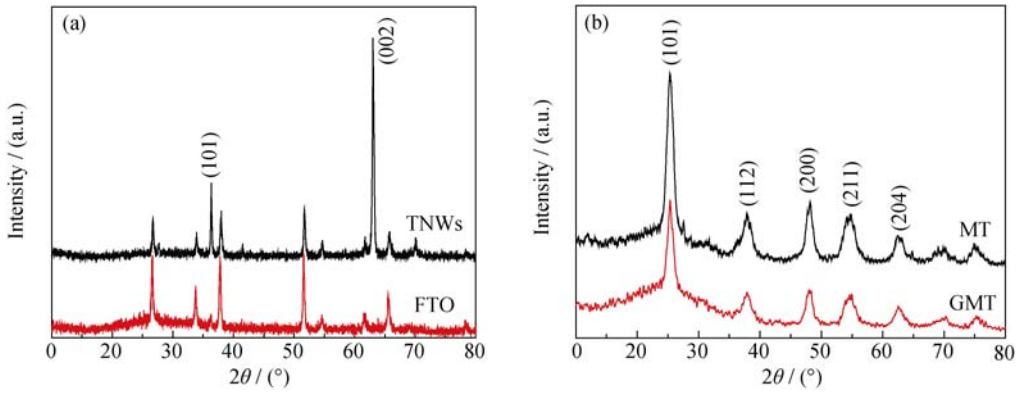

Fig. 2　XRD patterns of TNWs and FTO(a) , as well as MT and GMT composites (b)

favorable for high performance DSSCs. However, no clear diffraction peaks of graphene were observed in the composite films. This can be ascribed to that the most intense diffraction peak (002) of 3D graphene is largely overlapped by the anatase (101) peak, and its amount is too low[17, 28].

The existence of graphene in the composite was further confirmed by Raman spectra. As was shown in Fig. 3, graphene exhibits Raman shifts at 1577 and 1358 cm^{-1}, corresponding to the G (E_{2g} mode of sp^2 carbon atoms) and D bands (symmetry A_{1g} mode), respectively[29-30], indicating successful incorporation of graphene into the TiO_2 matrix. The relative weaker intensity of D peak than G peak and the existence of 2D peak in the spectra further revealed the high quality of the prepared specimens. The continuous planar structure and high electric conductivity endows the graphene a great electron transport channel to bridge the mesoporous TiO_2 particles. Figure S2 depicts the N_2 adsorption-desorption isotherm and pore size distribution of TNWs/GMT. The isotherm exhibits typical type IV pattern with hysteresis loop, a typical characteristic of mesoporous materials according to the classification of IUPAC[31]. A sharp increase in adsorption volume of N_2 was observed between 0.5–0.7 of relative partial pressure. This sharp increase can be attributed to the capillary condensation, indicating a good homogeneity of the sample. The BJH pore size distribution obtained from the desorption branch of the isotherms appears to be narrow (see inset of Fig. S3). The specific surface area of TNWs/GMT calculated using Barrett-Joyner-Halenda (BJH) method was found to be 129 m^2/g, three times higher than that of P25 powder (50 m^2/g) and certainly among the highest found in the literature for titania powder after calcination[32]. Such porous structures with relatively high specific surface area could be extremely useful for solar cells, as they would provide more sites for the absorption of dye molecules.

Electrochemical impedance spectroscopy (EIS) was used to compare the ion-transport behavior and electrical resistance of the bare TNWs, TNWs/MT and TNWs/GMT films, as shown in Fig. 4(a). In the high-frequency and middle-frequency regions, two semicircles can be seen in all curves. The former reflects the impedance of the charge transfer process at the counter electrode, while the latter is related to the charge transport process at the photoanode- electrolyte interface[33-36]. The equivalent circuit of the DSSCs is shown as an inset of Fig. 4(a). The Z_w, CPE, R_s, R_{ct1} (R_{ct2}) represent Warburg impedance, double-layer capacitance of the interface, series resistance, charge-transfer resistance between electrolyte and counter electrode (photoanode), respectively. Obviously, the second semicircles of TNWs/GMT is much smaller than the other two samples, indicating that moderate graphene loading contributes to the reduction of charge transfer resistance at the TiO_2-dye-electrolyte interface. This is due to the 2D graphene facilitating interfacial charge transfer among MT, as well as between MT and TNWs, thus lowering the charge recombination. The smaller semicircle of TNWs/MT than bare TNWs further indicated that the introduction of anatase mesoporous TiO_2 can provide efficient transport pathways for the electrolyte molecules.

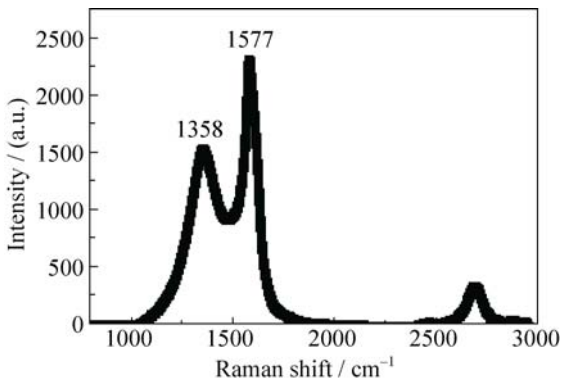

Fig. 3　Raman spectrum of GMT composites

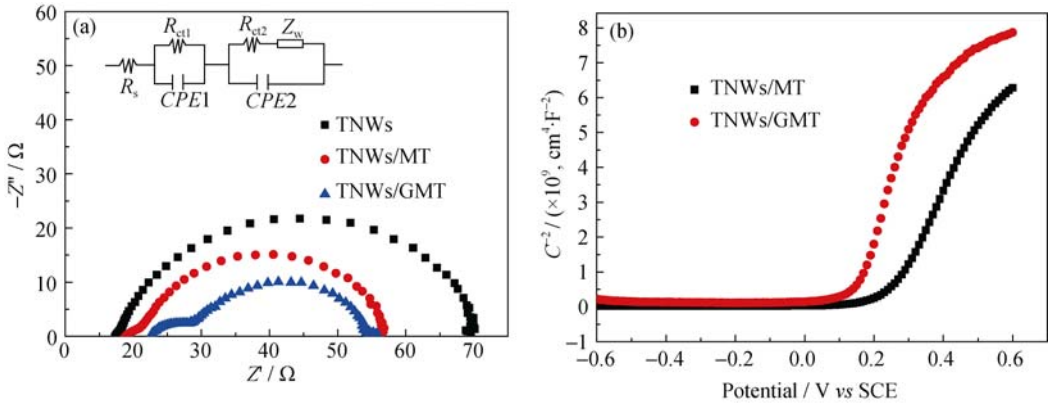

Fig. 4 Electrochemical impedance spectroscopy and electrical property (a) Nyquist plots of the impedance data of the DSSCs with anodes made of TNWs, TNWs/MT and TNWs/GMT. (b) Mott-Schottky patterns of TNWs/MT and TNWs/GMT

To investigate the electrical properties of TNWs/GMT and TNWs/MT samples, Mott-Schottky plots of both samples derived from electrochemical impedance measurements were shown in Fig. 4(b). The huge difference of slopes of the two plots indicates a wide gap of donor densities in TNWs/GMT and TNWs/MT. Carrier density was calculated from the slope using the following equation:

$$N_d = (2/e_0\varepsilon\varepsilon_0)\ [d(1/C^2)/dV]^{-1} \quad (1)$$

Where e_0, ε, ε_0, N_d, $d(1/C^2)/dV$ represent the electron charge, the dielectric constant of TiO_2[37], the permittivity of vacuum, the donor density and the straight slope, respectively. The calculated electron densities of TNWs/GMT and TNWs/MT are separately 1.28×10^{19} and 2.19×10^{19} cm^{-3}. This indicates that the graphene with favorable electrical conductivity could induces an exponential increase of electron density for the TNWs/GMT film, resulting in a faster carrier transfer than that in TNWs/MT film, and thus an enhanced DSSC performance. In addition, the flat band potential (E_{fb}) of the samples could be acquired by extrapolating the plots to $1/C^2 = 0$, giving an almost identical value of about –0.654 V for both TNWs/MT and TNWs/GMT films. As the open circuit voltage (V_{oc}) of a DSSC is determined by the difference between the redox potential of the electrolyte and E_{fb}[38], the equivalent E_{fb} suggests a similar V_{oc} of the TNWs/MT and TNWs/GMT based DSSCs, in accord with the cell performance presented in Fig. 5.

To investigate the photovoltaic performance of the DSSCs based on different photoanodes, the *J-V* curves are shown in Fig. 5, and the corresponding photovoltaic characteristics are summarized in Table 1. The overall efficiency (η) was evaluated using the equation $\eta = (FF \times J_{sc} \times V_{oc})/P_{in}$, where FF is the fill factor, J_{sc} is the short circuit current density, V_{oc} is the open-circuit voltage, and P_{in} is the incident light power density. The efficiency increased from 3.04% for bare TNWs to 6.00% for TNWs/MT, and further increased to 7.58% for TNWs/GMT. This improvement in energy conversion efficiency is due to the following reasons. Firstly, the infiltration of mesoporous TiO_2 significantly increased the specific surface area of the TNWs based film, which value is usually quite low due to their 1D morphology. As a result, the TNWs/MT composite with a larger specific surface area provide more sites for the absorption of dye molecules, thus leading to more photoinduced electrons being injected from the excited state of the dye into the conduction band of the TiO_2. Secondly, after graphene decorating, the photoinduced electrons can be easily transferred to the TNWs from MT (Scheme 1). The rapid transport of the photogenerated electrons in graphene not only reduces the recombination rate and resistance at the TiO_2-dye-electrolyte interface, but also bridged the electrons transportation inside MT matrix (Scheme 1).

In order to further confirm the role of graphene in DSSCs, incident monochromatic photo-to-electron conversion efficiency (IPCE) measurements were conducted. The maxima of the IPCE, at approximately 525 nm, is contributed to by the dye absorption, which corresponds to the visible $t_2 \rightarrow \pi^*$ metal-to-ligand charge transfer[23]. It is clear that the DSSC fabricated with TNWs/GMT photoanode shows highest IPCE value of 55%, while TNWs/MT and bare TNWs based photoanode show lower

Table 1 Solar cell parameters of cells*

Sample	V_{oc}	J_{sc} /(mA·cm^{-2})	Fill factor/%	Efficiency/%	Thickness/μm
TNWs	0.69	7.4	59	3.04	2.46
TNWs/MT	0.67	16.7	53	6.00	2.57
TNWs/GMT	0.67	18.3	61	7.58	2.59

* Exposed cell area: 0.15 cm^2, under 1 sun illumination (100 mW/cm^2) with the listed photoanode, and all cells with Pt/FTO as the counter electrode.

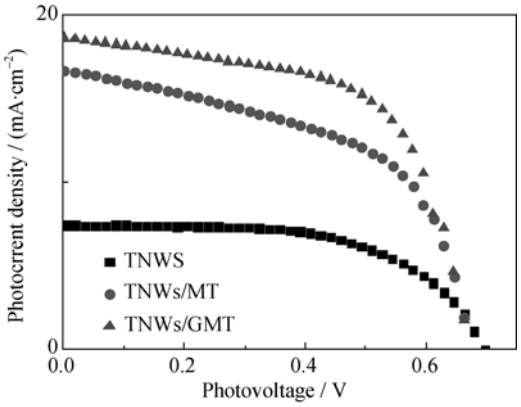

Fig. 5　*J-V* characteristics of DSSC solar cells with different photoanodes

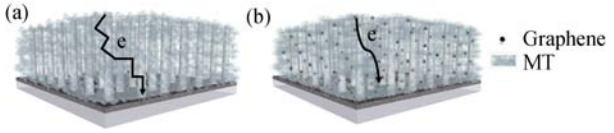

Scheme 1　Electron transport in TNWs/MT (a) and TNWs/GMT nanocomposites films cast on FTO (b)

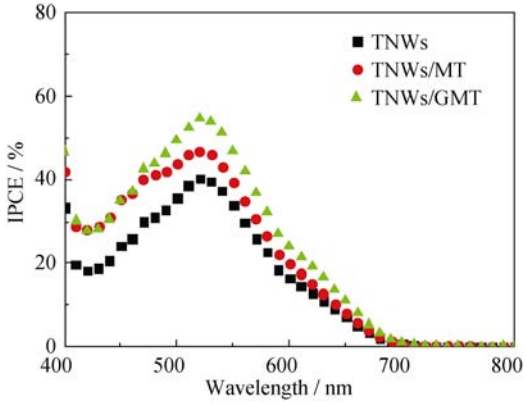

Fig. 6　IPCE curves of TNWs, TNWs/MT and TNWs/GMT

value of 47%, 40%, respectively. The enhanced IPCE value is ascribed to the higher specific surface areas and improved electron transfer abilities of the TNWs/ GMT materials, which results in a considerably higher dye molecule loading and enhanced charge collection at the electrode. On the other hand, the lower IPCE values in TNWs indicate that the electron-collection efficiency at the TiO_2/FTO substrate is poor due to the smaller surface area and lower dye absorption capacity of the materials[39]. Thus, the high IPCE of the DSSC fabricated with the TNWs/GMT photoanode results in a high photocurrent density and photovoltaic performance.

3　Conclusions

1D TNWs was infiltrated with graphene decorated mesoporous TiO_2 by multi-step EISA process. The pre pared TNWs/GMT and TNWs/MT hybrid photoanode material showed much higher efficiencies (7.58% and 6.00%, respectively) in dye-sensitized solar cells than the efficiency of the bare TNWs (3.04%). This results demonstrate that the introduction of mesoporous TiO_2 and graphene into 1D TNWs framework can not only significantly increase the specific surface area of photoanode, but also accelerates the electron transfer and reduces the charge recombination. The infiltration of graphene decorated nanocomposites in 1D TNWs may facilitate the fine-tuning of photoanode structures for further efficiency improvement of DSSCs.

References:

[1] OREGAN B, GRÄTZEL M. A low-cost, high-efficiency solar-cell based on dye-sensitized colloidal TiO_2 films. *Nature*, 1991, **353(6346):** 737–740.

[2] HAGFELDT A, GRÄTZEL M. Light-induced redox reactions in nanocrystalline systems. *Chem. Rev.*, 1995, **95(1):** 49–68.

[3] NAZEERUDDIN M K, KAY A, RODICIO I, *et al.* Conversion of light to electricity by Cis-X2bis(2,2'-Bipyridyl-4,4'-Dicarboxylate) ruthenium(Ii) charge-transfer sensitizers (X = Cl-, Br-, I-, Cn-, and Scn-) on nanocrystalline TiO_2 electrodes. *J. Am. Chem. Soc.*, 1993, **115(14):** 6382–6390.

[4] GRÄTZEL M. Recent advances in sensitized mesoscopic solar cells. *Accounts Chem. Res.*, 2009, **42(11):** 1788–1798.

[5] GRÄTZEL M. Dye-sensitized solar cells. *Journal of Photochemistry and Photobiology C: Photochemistry Reviews*, 2003, **4(2):** 145–153.

[6] PETER L M. Characterization and modeling of dye-sensitized solar cells. *J. Phys. Chem. C*, 2007, **111(18):** 6601–6612.

[7] SODERGREN S, HAGFELDT A, OLSSON J, *et al.* Theoretical-models for the action spectrum and the current-voltage characteristics of microporous semiconductor-films in photoelectrochemical cells. *J. Phys. Chem.-Us.*, 1994, **98(21):** 5552–5556.

[8] ZHANG J Y, TIAN H M, TIAN Z P *et al.* Study on sol-hydrothermal synthesis of TiO_2 nanoparticles and their photoelectric properties sensitized by dye. *J. Inorg. Mater.*, 2009, **24(6):** 1110–1114.

[9] VARGHESE O K, GONG D W, PAULOSE M, *et al.* Crystallization and high-temperature structural stability of titanium oxide nanotube arrays. *J. Mater. Res.*, 2003, **18(1):** 156–165.

[10] WANG H, BAI Y, WU Q, *et al.* Rutile TiO_2 nano-branched arrays on FTO for dye-sensitized solar cells. *Physical Chemistry Chemical Physics : PCCP*, 2011, **13(15):** 7008–7013.

[11] ZHU K, NEALE N R, MIEDANER A, *et al.*, Enhanced charge-collection efficiencies and light scattering in dye-sensitized solar cells using oriented TiO_2 nanotubes arrays. *Nano Letters*, 2007, **7(1):** 69–74.

[12] LUO H M, LIU Z Y, BAI C Y, *et al.* TiO_2 nanotube Based dye-sensitized photoanode. *J. Inorg. Mater.*, 2013, **28(5):** 521–526.

[13] CHEN W, QIU Y, YANG S. A new ZnO nanotetrapods/SnO_2 nanoparticles composite photoanode for high efficiency flexible dye-sensitized solar cells. *Physical Chemistry Chemical Physics : PCCP*, 2010, **12(32):** 9494–9501.

[14] HUO K F, WANG H R, ZHANG X M, *et al.* Heterostructured TiO_2 nanoparticles/nanotube arrays: *in situ* formation from amorphous TiO_2 nanotube arrays in water and enhanced photocatalytic activity. *Chempluschem*, 2012, **77(4):** 323–329.

[15] LIN J, LIU X, GUO M, *et al.* A facile route to fabricate an anodic

TiO_2 nanotube-nanoparticle hybrid structure for high efficiency dye-sensitized solar cells. *Nanoscale*, 2012, **4(16):** 5148–5153.

[16] QI L, YU H, LEI Z, *et al.* Dye-sensitized solar cells based on ZnO nanowire array/TiO_2 nanoparticle composite photoelectrodes with controllable nanowire aspect ratio. *Applied Physics A*, 2013, **111(1):** 279–284.

[17] FAN J, LIU S, YU J. Enhanced photovoltaic performance of dye-sensitized solar cells based on TiO_2 nanosheets/graphene composite films. *Journal of Materials Chemistry*, 2012, **22(33):** 17027–17036.

[18] YEN M Y, HSIAO M C, LIAO S H, *et al.* Preparation of graphene/multi-walled carbon nanotube hybrid and its use as photoanodes of dye-sensitized solar cells. *Carbon*, 2011, **49(11):** 3597–3606.

[19] ALLEN M J, TUNG V C, KANER R B. Honeycomb carbon: a review of graphene. *Chem. Rev.*, 2010, **110(1):** 132–145.

[20] XIANG Q, YU J, JARONIEC M. Enhanced photocatalytic H(2)-production activity of graphene-modified titania nanosheets. *Nanoscale*, 2011, **3(9):** 3670–3678.

[21] HUMMERS W S, OFFEMAN R E. Preparation of graphitic oxide. *J. Am. Chem. Soc.*, 1958, **80(6):** 1339.

[22] FENG X J, SHANKAR K, VARGHESE O K, *et al.* Vertically aligned single crystal TiO_2 nanowire arrays grown directly on transparent conducting oxide coated glass: synthesis details and applications. *Nano Letters*, 2008, **8(11):** 3781–3786.

[23] CHENG G, AKHTAR M S, YANG O B, *et al.*, Novel preparation of anatase TiO_2@reduced graphene oxide hybrids for high-performance dye-sensitized solar cells, *ACS Applied Materials & Interfaces*, 2013, **5(14):** 6635–6642.

[24] GRÄTZEL C, ZAKEERUDDIN S M. Recent trends in mesoscopic solar cells based on molecular and nanopigment light harvesters, *Mater Today*, 2013, **16(1/2):** 11–18.

[25] PARK N G, VAN DE LAGEMAAT J, FRANK A J. Comparison of dye-sensitized rutile- and anatase-based TiO_2 solar cells. *J. Phys. Chem. B*, 2000, **104(38):** 8989–8994.

[26] KALYANASUNDARAM K, GRÄTZEL M. Applications of functionalized transition metal complexes in photonic and optoelectronic devices. *Coordin. Chem. Rev.*, 1998, **177:** 347–414.

[27] WOLD A. Photocatalytic properties of TiO_2. *Chem. Mater.*, 1993, **5(3):** 280–283.

[28] YU J, MA T, LIU S. Enhanced photocatalytic activity of mesoporous TiO_2 aggregates by embedding carbon nanotubes as electron-transfer channel. *Physical Chemistry Chemical Physics : PCCP*, 2011, **13(8):** 3491–3501.

[29] FERRARI A C, MEYER J C, SCARDACI V, *et al.* Raman spectrum of graphene and graphene layers. *Physical Review Letters*, 2006, **97(18):** 187401–1–3.

[30] ZHU C, GUO S, WANG P, *et al.* One-pot, water-phase approach to high-quality graphene/TiO_2 composite nanosheets. *Chemical Communications*, 2010, **46(38):** 7148–7150.

[31] ALEXAKI N, STERGIOPOULOS T, KONTOS A G, *et al.*, Mesoporous titania nanocrystals prepared using hexadecylamine surfactant template: crystallization progress monitoring, morphological characterization and application in dye-sensitized solar cells, *Microporous and Mesoporous Materials*, 2009, **124(1/2/3):** 52–58.

[32] ZHANG R, ELZATAHRY A A, AL-DEYAB S S, *et al.* Mesoporous titania: from synthesis to application. *Nano Today*, 2012, **7(4):** 344–366.

[33] BI H, HUANG F, LIANG J, *et al.* Large-scale preparation of highly conductive three dimensional graphene and its applications in CdTe solar cells. *Journal of Materials Chemistry*, 2011, **21(43):** 17366–17370.

[34] BI H, SUN S, HUANG F, *et al.* Direct growth of few-layer graphene films on SiO_2 substrates and their photovoltaic applications. *Journal of Materials Chemistry*, 2012, **22(2):** 411–416.

[35] ZHI J, DENG S, ZHANG Y, *et al.* Embedding Co_3O_4 nanoparticles in SBA-15 supported carbon nanomembrane for advanced supercapacitor materials. *Journal of Materials Chemistry A*, 2013, **1(9):** 3171–3176.

[36] ZHI J, WANG Y F, DENG S, *et al.* Study on the relation between pore size and supercapacitance in mesoporous carbon electrodes with silica-supported carbon nanomembranes. *Rsc. Adv.*, 2014, **4(76):** 40296–40300.

[37] TANG H, PRASAD K, SANJINES R, *et al.* Electrical and optical-properties of TiO_2 anatase thin-films. *J. Appl. Phys.*, 1994, **75(4):** 2042–2047.

[38] DUAN Y D, FU N Q, LIU Q P, *et al.* Sn-doped TiO_2 photoanode for dye-sensitized solar cells. *J. Phys. Chem. C*, 2012, **116(16):** 8888–8893.

[39] SUN S, GAO L, LIU Y. Enhanced dye-sensitized solar cell using graphene-TiO_2 photoanode prepared by heterogeneous coagulation. *Applied Physics Letters*, 2010, **96(8):** 083113–1–3.

基于介孔 TiO_2/石墨烯修饰的 TiO_2 纳米线光阳极的染料敏化太阳能电池

陈盎然[1]，赵 伟[1]，崔厚磊[1]，支 键[1]，黄富强[1, 2]

(1. 中国科学院能量转换材料重点实验室，中国科学院 上海硅酸盐研究所，上海 200050；2. 北京分子科学国家实验室，北京 100871)

摘 要: 本工作制作了基于介孔 TiO_2/石墨烯修饰的 TiO_2 纳米线光阳极的染料敏化太阳能电池，并进行表征。光阳极结合了介孔 TiO_2 的高染料吸附率，TiO_2 纳米线的高载流子传导率和石墨烯的高电子收获能力等优点，使器件光电转换效率有了很大的提高。制作出的染料敏化太阳能电池光电转换效率高达 7.58%，比纯纳米线制作的电池约提高了 1.5 倍，在拥有相似一维结构的染料敏化太阳能电池中具有较大优势。

关 键 词: 掺染料敏化太阳能电池；TiO_2 纳米线；介孔 TiO_2；石墨烯

中图分类号: TQ174 **文献标识码:** A

Supporting Information

TiO_2 Nanowires Infiltrated with Graphene-decorated Mesoporous TiO_2 for Enhanced Dye-sensitized Solar Cell

CHEN Ang-Ran[1], ZHAO Wei[1], CUI Hou-Lei[1], ZHI Jian[1], HUANG Fu-Qiang[1, 2]

(1. CAS Key Laboratory of Materials for Energy Conversion, Shanghai Institute of Ceramics, Chinese Academy of Sciences, Shanghai 200050, China; 2. Beijing National Laboratory for Molecular Sciences, Beijing 100871, China)

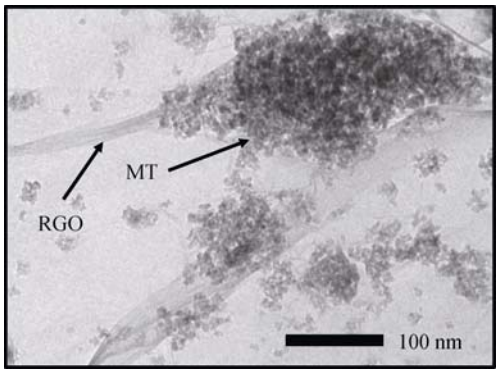

Fig. S1　TEM image of GMT

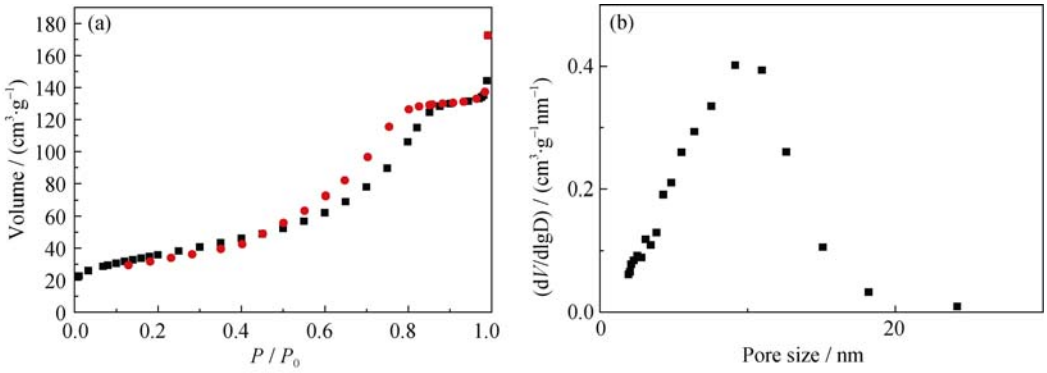

Fig. S2　N_2 desorption and adsorption of TNWs/GMT

Experimental section support information:

Materials:

Titanium tetraisopropoxide and absolute ethanol were all of A.R grade and were all purchased from Aladdin Chemical Reagent Co., Ltd, China. Sensitized dye N719 (RuL_2 $(NCS)_2$, L=4,4'-dicarboxylate-2,2' -bipyridine) was purchased from Solaronix SA (Switzerland). F127 ($EO_{106}PO_{70}EO_{106}$) was purchased from Sigma-Aldrich. All reagents were used without further treatment. Indium-tin Oxide/poly (ethylene terephthalate) (ITO/PET, 60 Ω, from IST/USA) was used as a substrate for DSSC test.

Fabrication of DSSCs

The obtained anode thin film deposited on FTO glass was immersed into a 0.05 mol/L $TiCl_4$ aqueous solution at 70℃ and kept for 30 min to improve the photocurrent and photovoltaic performances. After sintering at 450℃ for 30 min, the film was sensitized by a 2.5×10^{-4} mol/L N719 absolute ethanol solution for 24 h to adsorb the dye adequately. Then, the electrode was sandwiched together with a platinized FTO counter electrode. The redox electrolyte was injected into the aperture between the dye sensitized TiO_2 film electrode and the counter electrode.

Measurements and characterization:

XRD measurements were carried out using powder X-ray diffraction (Bruker D8 Advance, with Cu_KR radiation operating at 40 kV and 40 mA, scanning from 2θ=20° to 80°). Field emission scanning electron microscopy (FESEM; Hitachi S-4800) and transmission electron microscope (JEOL 2100 TEM, 200 kV) was used to characterize the morphology of the films. Nitrogen adsorption desorption isotherms for surface area and pore analyses were

measured using a Nova 3200e (Quantachrome instruments). Raman spectra were recorded at room temperature using a micro-Raman spectrometer (InVia, Renishaw PLC, Gloucestershire, UK) with backscattering geometry, using a 514.5 nm Ar+ laser as an excitation source. The amount of adsorbed dye was measured by desorbing the dye into 20 mmol/L NaOH solution with equal amount of deionized water and ethanol and by absorption measurement of the solution using the absorption peak intensity of N719 at 511 nm. The current voltage test of DSSCs were performed under one sun condition using a solar light simulator (Oriel, 91160, AM 1.5 globe,100 mW/cm^2). The incident-light intensity was calibrated using a radiant power/energy meter (Oriel, 70260) before each experiment. The incident-photonto-current conversion efficiency (IPCE) spectra were measured using a specially designed IPCE system (Newport Co., USA). Electrochemical impedance spectroscopy (EIS) measurements were performed on a computer- ontrolled electrochemical workstation with impedance analyzer (CHI660C Instruments, Shanghai Chenhua Instrument Corp., Shanghai, China). The measurements were carried out by applying bias of the open circuit voltage (V_{oc}) and were recorded over a frequency range of 0.005 to 105 Hz with AC amplitude of 10 mV. The transient photocurrent curves were measured using an electrochemical analyzer (CHI660C Instruments, Shanghai Chenhua Instrument Corp., Shanghai, China) controlled by a computer. The light was produced by a solar simulator (91160, Newport Corp., Irvine, CA, USA) at 100 mW/cm^2 (1 sun) intensity.